SIAM J. SCI. COMPUT.
Vol. 19, No. 4, pp. 1169–1187, July 1998
© 1998 Society for Industrial and Applied Mathematics
007

A CHARGE SIMULATION METHOD FOR NUMERICAL CONFORMAL MAPPING ONTO CIRCULAR AND RADIAL SLIT DOMAINS*

KANAME AMANO†

Abstract. A simple numerical method is described for computing the following two conformal maps: (a) from a domain exterior to closed Jordan curves onto a circular slit domain and (b) from a domain exterior to closed Jordan curves onto a radial slit domain. They constitute a dual problem and can be computed in a dual way. The numerical method is based on the charge simulation method or the method of fundamental solutions applied to the Dirichlet problem of Laplace's equation in which a pair of conjugate harmonic functions are approximated by a linear combination of complex logarithmic potentials. The unknown coefficients are determined by the collocation condition imposed on the real part or the imaginary part, the modulus or the argument, of the approximate mapping function. Effectiveness of the method is demonstrated by some typical examples.

Key words. numerical conformal mapping, circular slits, radial slits, charge simulation method, fundamental solution

AMS subject classifications. 30C30, 65E05

PII. S1064827595294307

1. Introduction.

Conformal mapping is a fundamental subject in complex analysis and is familiar in science and engineering. However, exact mapping functions are known only for special domains. Numerical mapping has been an important subject of numerical analysis.

We are concerned here with the following two types of conformal mapping: (a) from a domain exterior to closed Jordan curves onto a circular slit domain and (b) from a domain exterior to closed Jordan curves onto a radial slit domain. The circular slit domain is the entire plane with slits along the concentric circular arcs whose common center is the origin. The mapping onto the circular slit domain is important in problems of two-dimensional vortex flow with obstacles. The radial slit domain is the entire plane with slits along the rectilinear lines pointing at the origin. The mapping onto the radial slit domains is important in problems of two-dimensional point-source flow with obstacles. However, until quite recently, a suitable method had not been proposed for computing these maps, especially for computing the map onto domains with rectilinear slits.

Symm [27, 28, 29] proposed well-known integral equation methods for computing conformal maps from interior, exterior, and doubly connected Jordan domains onto the unit disk, its exterior, and a circular annulus, respectively. A pair of conjugate harmonic functions are expressed by a complex single-layer logarithmic potential, and the mapping problems are reduced to singular Fredholm integral equations of the first kind. He approximated the unknown source density by a step function. Gaier [10, 11] mathematically studied Symm's integral equation and proved the existence and uniqueness of the solution. Hayes, Kahaner, and Kellner [12] approximated the source density by a piecewise quadratic polynomial and improved the accuracy of the numerical results. Hough and Papamichael [15, 16] approximated the source density

* Received by the editors November 1, 1995; accepted for publication (in revised form) August 21, 1996; published electronically April 16, 1998.
http://www.siam.org/journals/sisc/19-4/29430.html
† Department of Computer Science, Faculty of Engineering, Ehime University, Matsuyama 790, Japan (amano@cs.ehime-u.ac.jp).

Downloaded 11/05/25 to 185.230.125.55 . Redistribution subject to SIAM license or copyright; see https://epubs.siam.org/terms-privacy

by spline functions and singular functions and overcame the difficulties associated with corner singularities. They also reformulated Symm's methods, based on the derivation of Gaier [10, 11], into a unified method for the numerical conformal mapping of the interior, exterior, and doubly connected domains. These methods need $O(N^3)$ operations if the boundary is discretized at N points. On the other hand, Henrici [13], Berrut [7], and Reichel [26] modified Symm's methods to incorporate some iteration procedures and obtained $O(N^2 \log N)$ solutions by means of the fast Fourier transform. See [9, 14, 30] for surveys of numerical conformal mapping.

Amano [1–4] proposed the charge simulation method or the method of fundamental solutions for the numerical conformal mapping of the interior, exterior, and doubly connected Jordan domains. The conjugate harmonic functions are approximated by a linear combination of complex logarithmic potentials, and the mapping problems are reduced to a set of simultaneous linear equations. The method is quite simple though it has a potentially large number of free parameters. If the domains have no reentrant corners, the method can give numerical results of high accuracy using, without integration, rather fewer discretization points than Symm's original integral equation methods. Recently, Amano [5, 6] applied the charge simulation method to the problems of conformal mapping at issue here, i.e., (a) from a domain exterior to closed Jordan curves onto the circular slit domain and (b) from a domain exterior to closed Jordan curves onto the radial slit domain. The results were successful.

In this paper, the two methods [5, 6] are reformulated into a unified method for the numerical conformal mapping onto the circular slit domain and onto the radial slit domain. The original formulations are not repeated. The two problems constitute a dual problem and can be computed in a dual way. The difference is that the unknown coefficients are determined by the collocation condition imposed on the real part or the imaginary part, the modulus or the argument, of the mapping function. The effectiveness of the method is demonstrated by some typical examples.

2. Charge simulation method. An outline of the charge simulation method is given in advance. Consider the two-dimensional Laplace equation

$$\Delta g(z) = 0 \quad \text{in } D \tag{2.1}$$

with the boundary condition

$$g(z) = b(z) \quad \text{on } C, \tag{2.2}$$

where D is a domain with its boundary C, and $b(z)$ is a function defined on C. The notation $g(z)$ is an abbreviation of $g(x, y)$, where $z = x + iy$.

The charge simulation method approximates the solution that is continuous in $\bar{D} = D \cup C$ by

$$G(z) = \sum_{i=1}^{N} Q_i \log |z - \zeta_i|, \tag{2.3}$$

namely, a linear combination of logarithmic potentials or fundamental solutions of the Laplace operator. The singular points $\zeta_1, \ldots, \zeta_N \notin \bar{D}$, which are called the *charge points*, are arranged outside the given domain. The unknown constants $Q_1, \ldots, Q_N$, which are called the *charges*, are determined to satisfy the boundary condition (2.2) at the collocation points $z_1, \ldots, z_N \in C$ arranged on the boundary. That is to say

Downloaded 11/05/25 to 185.230.125.55 . Redistribution subject to SIAM license or copyright; see https://epubs.siam.org/terms-privacy

Downloaded 11/05/25 to 185.230.125.55 . Redistribution subject to SIAM license or copyright; see https://epubs.siam.org/terms-privacy

they are solutions of a system of simultaneous linear equations

$$\sum_{i=1}^{N} Q_i \log|z_j - \zeta_i| = b(z_j), \quad j = 1, \ldots, N, \tag{2.4}$$

which are called the *collocation conditions*. Once $Q_1, \ldots, Q_N$ are determined, $g(z)$ can be approximated by $G(z)$ at any point in $\bar{D}$.

The approximation $G(z)$ exactly satisfies the Laplace equation (2.1). Consequently, if the domain D is bounded, from the maximum principle for harmonic functions the computational error can be estimated as

$$E_G(z) = |G(z) - g(z)| \leq \max_{C} |G(z) - b(z)| = E_G; \tag{2.5}$$

that is, $E_G(z)$ takes its maximum value E_G somewhere on the boundary. Furthermore, from the collocation condition (2.4), E_G can be estimated as

$$E_G \simeq \max_{j} |G(z_{j+1/2}) - b(z_{j+1/2})|, \tag{2.6}$$

where $z_{j+1/2} \in C$ is an intermediate point between the successive collocation points z_j and z_{j+1}. It is known that, if the boundary curve and the data are analytic, the charge simulation method can give an approximation of exponentially small error with respect to N.

Mathon and Johnston [22] obtained crude results concerning error bounds and convergence of the method. Fairweather and Johnston [8] interpreted it as a discrete single-layer potential method using an auxiliary boundary. Katsurada and Okamoto [20] and Katsurada [17] obtained extensive results concerning error bounds and convergence of the method in such special domains as a disk, its exterior, or an annulus. Katsurada [18, 19] generalized the results to Jordan domains from a similar viewpoint as presented in [8]. Kitagawa [21] analyzed the numerical stability of the method. See [23, 25] for surveys of the charge simulation method.

3. Problems. Consider, as shown in Fig. 3.1, the conformal mapping of a domain D exterior to closed Jordan curves $C_1, \ldots, C_n$ in the z-plane including the point at infinity onto a circular slit domain. It is the entire w-plane with slits along concentric circular arcs whose common center is the origin. Assume that the origin $z = 0$ lies in D. Then the mapping function $w = f_c(z)$ is uniquely determined by the normalizing conditions $f_c(0) = 0$, $f_c(\infty) = \infty$, and $f_c'(\infty) = 1$. As a result, $C_1, \ldots, C_n$ are mapped onto the circular slits $S_{c1}, \ldots, S_{cn}$ with radii $r_1, \ldots, r_n$, respectively. See [24] for a survey of conformal mapping of multiply-connected domains.

The contour lines of $|f_c(z)|$ and $\arg f_c(z)$ are streamlines and equipotential lines of a two-dimensional vortex flow with obstacles, where a vortex is at the origin and $C_1, \ldots, C_n$ are outlines of the obstacles.

We express the mapping function as

$$f_c(z) = z \exp(g_c(z) + i h_c(z)) \quad \text{in } \bar{D}, \tag{3.1}$$

where $g_c(z)$ and $h_c(z)$ are conjugate harmonic functions in $\bar{D}$. The $g_c(z)$ should satisfy the boundary condition $|f_c(z)| = r_l$ on C_l; i.e.,

$$g_c(z) + \log|z| = \log r_l \quad \text{on } C_l, \quad l = 1, \ldots, n, \tag{3.2}$$

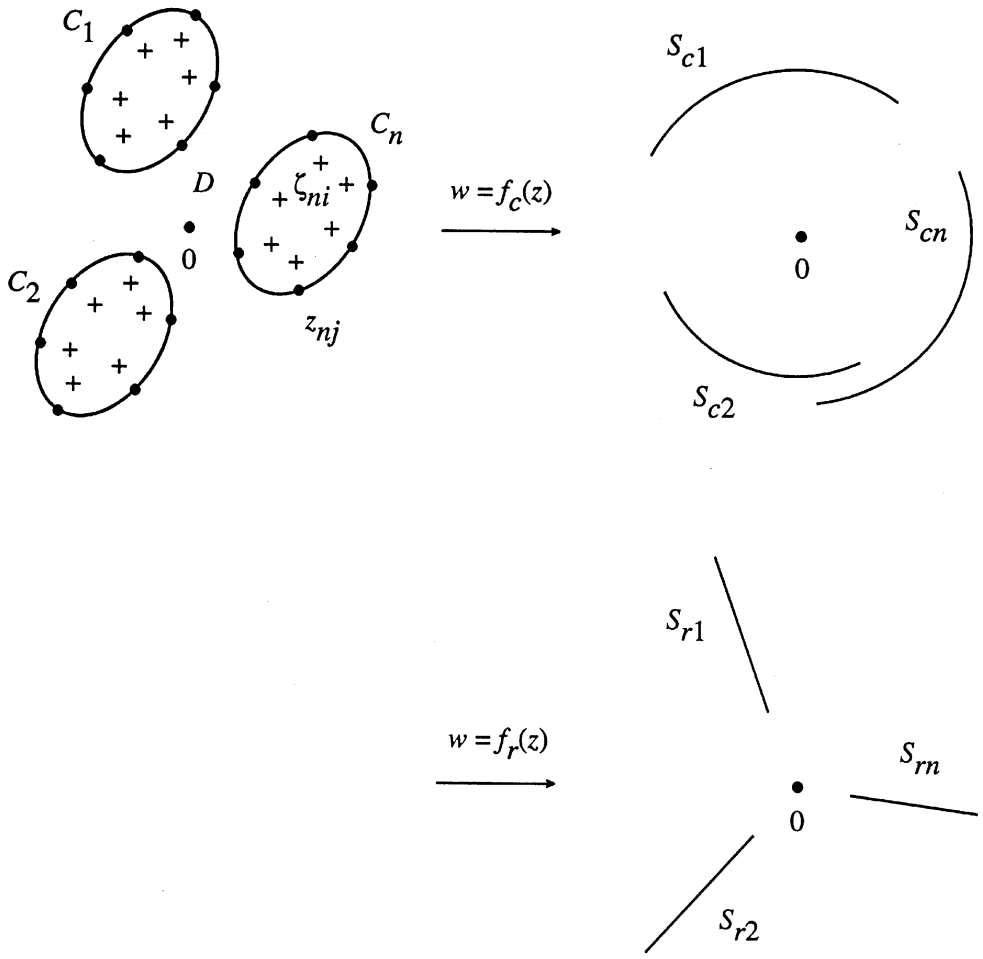

FIG. 3.1. *Conformal mapping and the charge simulation method.*

because $C_1, \ldots, C_n$ are mapped onto $S_{c1}, \ldots, S_{cn}$, respectively. From the condition at infinity, $f_c'(\infty) = \lim_{z\to\infty} f_c(z)/z = 1$; i.e.,

$$g_c(\infty) = h_c(\infty) = 0 \tag{3.3}$$

should be satisfied. Conversely, if (3.2) and (3.3) are satisfied, (3.1) is the mapping function of the problem. From the uniqueness of the solution, the mapping is now reduced to the problem of finding the conjugate harmonic functions $g_c(z)$ and $h_c(z)$.

Next, consider the conformal mapping of the same domain D onto a radial slit domain. It is the entire w-plane with slits along rectilinear lines pointing at the origin. Then the mapping function $w = f_r(z)$ is uniquely determined by the same normalizing conditions $f_r(0) = 0$, $f_r(\infty) = \infty$, and $f_r'(\infty) = 1$. As a result, $C_1, \ldots, C_n$ are mapped onto the radial slits $S_{r1}, \ldots, S_{rn}$ with arguments $\theta_1, \ldots, \theta_n$, respectively.

The contour lines of $|f_r(z)|$ and $\arg f_r(z)$ are equipotential lines and streamlines of a two-dimensional point-source flow with obstacles, where a point-source is at the origin and $C_1, \ldots, C_n$ are outlines of the obstacles.

Downloaded 11/05/25 to 185.230.125.55 . Redistribution subject to SIAM license or copyright; see https://epubs.siam.org/terms-privacy

Downloaded 11/05/25 to 185.230.125.55 . Redistribution subject to SIAM license or copyright; see https://epubs.siam.org/terms-privacy

We also express the mapping function as

$$f_r(z) = z \exp(g_r(z) + i h_r(z)) \quad \text{in } \bar{D}, \tag{3.4}$$

where $g_r(z)$ and $h_r(z)$ are conjugate harmonic functions in $\bar{D}$. The function $h_r(z)$ should satisfy the boundary condition $\arg f_r(z) = \theta_l$ on C_l; i.e.,

$$h_r(z) + \arg z = \theta_l \quad \text{on } C_l, \quad l = 1, \ldots, n, \tag{3.5}$$

because $C_1, \ldots, C_n$ are mapped onto $S_{r1}, \ldots, S_{rn}$, respectively. From the condition at infinity, $f_r'(\infty) = \lim_{z\to\infty} = f_r(z)/z = 1$; i.e.,

$$g_r(\infty) = h_r(\infty) = 0 \tag{3.6}$$

should be satisfied. Conversely, if (3.5) and (3.6) are satisfied, (3.4) is the mapping function of the problem. From the uniqueness of the solution, the mapping is now reduced to the problem of finding the conjugate harmonic functions $g_r(z)$ and $h_r(z)$.

Strictly speaking, in (3.3) and (3.6), $h_c(z)$ and $h_r(z)$ are determined only up to the addition of $2k\pi$ for any integer k. This corresponds to branches of $\log z$.

4. Numerical conformal mapping.

4.1. Mapping onto a circular slit domain. Based on the charge simulation method, the conjugate harmonic functions $g_c(z)$ and $h_c(z)$ can be approximated by a linear combination of complex logarithmic potentials

$$G_c(z) + i H_c(z) = \sum_{l=1}^{n} \sum_{i=1}^{N_l} Q_{li} \log(z - \zeta_{li}), \tag{4.1}$$

where N_l charge points $\zeta_{l1}, \ldots, \zeta_{lN_l}$ are arranged inside the domain bounded by C_l as shown in Fig. 3.1. Then a simple approximate mapping function

$$F_c(z) = z \exp(G_c(z) + i H_c(z)) \tag{4.2}$$

is obtained. The unknown charges $Q_{11}, Q_{12}, \ldots, Q_{nN_n}$ are determined to satisfy the boundary condition (3.2) at the same number of collocation points arranged on the boundary, i.e., N_l collocation points $z_{l1}, \ldots, z_{lN_l}$ on C_l. That is to say they should satisfy the simultaneous linear equations

$$\begin{gathered} \sum_{l=1}^{n} \sum_{i=1}^{N_l} Q_{li} \log |z_{mj} - \zeta_{li}| - \log R_m = -\log |z_{mj}|, \\ z_{mj} \in C_m, \quad j = 1, \ldots, N_m, \quad m = 1, \ldots, n. \end{gathered} \tag{4.3}$$

R_m is an approximation to r_m. From the condition at infinity (3.3),

$$\lim_{z\to\infty} \sum_{l=1}^{n} \sum_{i=1}^{N_l} Q_{li} \log(z - \zeta_{li}) = 0;$$

i.e.,

$$\sum_{l=1}^{n} \sum_{i=1}^{N_l} Q_{li} = 0 \tag{4.4}$$

Downloaded 11/05/25 to 185.230.125.55 . Redistribution subject to SIAM license or copyright; see https://epubs.siam.org/terms-privacy

should be satisfied. Furthermore, since the imaginary part of (4.1) should be single-valued in $\bar{D}$,

$$\int_{\tilde{C}} dH_c(z) = 0$$

for any closed contour $\tilde{C}$ lying in D. This is equivalent to

$$\begin{aligned}\int_{\tilde{C}_l} dH_c(z) &= \int_{\tilde{C}_l} d \sum_{m=1}^{n} \sum_{i=1}^{N_m} Q_{mi} \arg(z-\zeta_{mi}) \\ &= \sum_{i=1}^{N_l} Q_{li} \int_{\tilde{C}_l} d\arg(z-\zeta_{li}) + \sum_{m=1,\neq l}^{n} \sum_{i=1}^{N_m} Q_{mi} \int_{\tilde{C}_l} d\arg(z-\zeta_{mi}) \\ &= 2\pi \sum_{i=1}^{N_l} Q_{li} \\ &= 0;\end{aligned}$$

i.e.,

$$\sum_{i=1}^{N_l} Q_{li} = 0, \quad l = 1, \ldots, n, \tag{4.5}$$

where $\tilde{C}_l$ is an arbitrary closed contour lying in D and surrounding only C_l. Equations (4.4) and (4.5) are not independent; the latter implies the former.

Equations (4.3) and (4.5) constitute $N_1+\cdots+N_n+n$ simultaneous linear equations for $N_1 + \cdots + N_n + n$ unknowns $Q_{11}, Q_{12}, \ldots, Q_{nN_n}, \log R_1, \ldots, \log R_n$. Once they are determined, $F_c(z)$ can be computed by (4.1) and (4.2) at any point in $\bar{D}$.

$H_c(z)$ should be not only single valued but also continuous in $\bar{D}$. For computation, we use the principal value of logarithmic function. However, if arg is simply replaced by Arg, then the function

$$H_c(z) = \sum_{l=1}^{n} \sum_{i=1}^{N_l} Q_{li} \mathrm{Arg}(z-\zeta_{li}) \tag{4.6}$$

is not continuous in $\bar{D}$, because $\mathrm{Arg}\, z$ has the 2π discontinuity on the negative real axis. Therefore, substituting (4.5), we change (4.1) to

$$\begin{aligned}G_c(z) + iH_c(z) = \sum_{l=1}^{n} \Bigg\{ &\sum_{i=1}^{N_l-1} \left(\sum_{k=1}^{i} Q_{lk} \right) (\log(z-\zeta_{li}) - \log(z-\zeta_{l,i+1})) \\ &+ \left(\sum_{k=1}^{N_l} Q_{lk} \right) \log(z-\zeta_{lN_l}) \Bigg\} \\ = \sum_{l=1}^{n} \sum_{i=1}^{N_l-1} &\left(\sum_{k=1}^{i} Q_{lk} \right) \log \left(\frac{z-\zeta_{li}}{z-\zeta_{l,i+1}} \right)\end{aligned} \tag{4.7}$$

and take its principal value. The imaginary part

$$H_c(z) = \sum_{l=1}^{n} \sum_{i=1}^{N_l-1} \left(\sum_{k=1}^{i} Q_{lk} \right) \mathrm{Arg} \left(\frac{z-\zeta_{li}}{z-\zeta_{l,i+1}} \right) \tag{4.8}$$

Downloaded 11/05/25 to 185.230.125.55 . Redistribution subject to SIAM license or copyright; see https://epubs.siam.org/terms-privacy

can now be continuous in $\bar{D}$ if charges are so arranged that the straight line connecting ζ_{li} and $\zeta_{l,i+1}$ does not intersect C_l, because discontinuity of $\mathrm{Arg}((z-\zeta_{li})/(z-\zeta_{l,i+1}))$ appears on the line connecting ζ_{li} and $\zeta_{l,i+1}$. The linear equations (4.3) can also be changed to

$$\sum_{l=1}^{n}\sum_{i=1}^{N_l-1}\left(\sum_{k=1}^{i}Q_{lk}\right)\log\left|\frac{z_{mj}-\zeta_{li}}{z_{mj}-\zeta_{l,i+1}}\right|-\log R_m=-\log|z_{mj}|,$$

$$z_{mj}\in C_m,\quad j=1,\dots,N_m,\quad m=1,\dots,n. \tag{4.9}$$

The formulation described above is summarized as follows.

Formulation CSLIT1. The approximate mapping function is given by

$$F_c(z)=z\exp(G_c(z)+iH_c(z)),$$

$$\begin{aligned}G_c(z)+iH_c(z)&=\sum_{l=1}^{n}\sum_{i=1}^{N_l-1}Q_l^i\,\mathrm{Log}\left(\frac{z-\zeta_{li}}{z-\zeta_{l,i+1}}\right)\\&=\sum_{l=1}^{n}\sum_{i=1}^{N_l-1}Q_l^i\left\{\log\left|\frac{z-\zeta_{li}}{z-\zeta_{l,i+1}}\right|+i\mathrm{Arg}\left(\frac{z-\zeta_{li}}{z-\zeta_{l,i+1}}\right)\right\},\end{aligned}$$

where the unknown constants $Q_l^i=\sum_{k=1}^{i}Q_{lk}$, $i=1,\dots,N_l-1$, $l=1,\dots,n$ and $\log R_1,\dots,\log R_n$ are solutions of the $N_1+\cdots+N_n$ simultaneous linear equations

$$\sum_{l=1}^{n}\sum_{i=1}^{N_l-1}Q_l^i\log\left|\frac{z_{mj}-\zeta_{li}}{z_{mj}-\zeta_{l,i+1}}\right|-\log R_m=-\log|z_{mj}|,$$

$$z_{mj}\in C_m,\quad j=1,\dots,N_m,\quad m=1,\dots,n.$$

If $C_1,\dots,C_n$ are starlike with respect to their inside points $z_{10},\dots,z_{n0}$, also using (4.5) we can change (4.1) to

$$\begin{aligned}G_c(z)+iH_c(z)&=\sum_{l=1}^{n}\sum_{i=1}^{N_l}Q_{li}\log(z-\zeta_{li})-\sum_{l=1}^{n}\sum_{i=1}^{N_l}Q_{li}\log(z-z_{l0})\\&=\sum_{l=1}^{n}\sum_{i=1}^{N_l}Q_{li}\log\left(\frac{z-\zeta_{li}}{z-z_{l0}}\right)\end{aligned} \tag{4.10}$$

and take its principal value. The imaginary part

$$H_c(z)=\sum_{l=1}^{n}\sum_{i=1}^{N_l}Q_{li}\mathrm{Arg}\left(\frac{z-\zeta_{li}}{z-z_{l0}}\right) \tag{4.11}$$

is now continuous in $\bar{D}$, because discontinuity of $\mathrm{Arg}((z-\zeta_{li})/(z-z_{l0}))$ appears on the straight line connecting ζ_{li} and z_{l0}. Then another formulation can be obtained.

Formulation CSLIT2. The approximate mapping function is given by

$$F_c(z)=z\exp(G_c(z)+iH_c(z)),$$

$$G_c(z) + iH_c(z) = \sum_{l=1}^{n}\sum_{i=1}^{N_l} Q_{li}\mathrm{Log}\left(\frac{z-\zeta_{li}}{z-z_{l0}}\right)$$
$$= \sum_{l=1}^{n}\sum_{i=1}^{N_l} Q_{li}\left\{\log\left|\frac{z-\zeta_{li}}{z-z_{l0}}\right| + i\mathrm{Arg}\left(\frac{z-\zeta_{li}}{z-z_{l0}}\right)\right\},$$

where the unknown constants $Q_{11}, Q_{12}, \ldots, Q_{nN_n}$ and $\log R_1, \ldots, \log R_n$ are solutions of the $N_1 + \cdots + N_n + n$ simultaneous linear equations

$$\sum_{l=1}^{n}\sum_{i=1}^{N_l} Q_{li}\log\left|\frac{z_{mj}-\zeta_{li}}{z_{mj}-z_{l0}}\right| - \log R_m = -\log|z_{mj}|,$$

$$z_{mj} \in C_m, \quad j = 1, \ldots, N_m, \quad m = 1, \ldots, n,$$

$$\sum_{i=1}^{N_l} Q_{li} = 0,$$

$$l = 1, \ldots, n.$$

4.2. Mapping onto a radial slit domain. Similar to the case of circular slit domain, the conjugate harmonic functions $g_r(z)$ and $h_r(z)$ can be approximated by a linear combination of complex logarithmic potentials

$$G_r(z) + iH_r(z) = \sum_{l=1}^{n}\sum_{i=1}^{N_l} Q_{li}\log(z-\zeta_{li}), \tag{4.12}$$

and a simple approximate mapping function

$$F_r(z) = z\exp(G_r(z) + iH_r(z)) \tag{4.13}$$

is obtained. The unknown charges $Q_{11}, Q_{12}, \ldots, Q_{nN_n}$ are determined to satisfy the boundary condition (3.5) at the collocation points on the boundary. That is to say they should satisfy the simultaneous linear equations

$$\sum_{l=1}^{n}\sum_{i=1}^{N_l} Q_{li}\arg(z_{mj}-\zeta_{li}) - \Theta_m = -\arg z_{mj},$$
$$z_{mj} \in C_m, \quad j = 1, \ldots, N_m, \quad m = 1, \ldots, n. \tag{4.14}$$

Θ_m is an approximation to θ_m. The charge points ζ_{li} and the collocation points z_{mj} can be the same as used for $F_c(z)$. From the condition at infinity (3.6) and from the single valuedness of (4.12) in $\bar{D}$,

$$\sum_{l=1}^{n}\sum_{i=1}^{N_l} Q_{li} = 0 \tag{4.15}$$

and

$$\sum_{i=1}^{N_l} Q_{li} = 0, \quad l = 1, \ldots, n, \tag{4.16}$$

Downloaded 11/05/25 to 185.230.125.55 . Redistribution subject to SIAM license or copyright; see https://epubs.siam.org/terms-privacy

Downloaded 11/05/25 to 185.230.125.55 . Redistribution subject to SIAM license or copyright; see https://epubs.siam.org/terms-privacy

are also obtained. Equation (4.16) implies (4.15).

Equations (4.14) and (4.16) constitute $N_1 + \cdots + N_n + n$ simultaneous linear equations for $N_1 + \cdots + N_n + n$ unknowns $Q_{11}, Q_{12}, \ldots, Q_{nN_n}, \Theta_1, \ldots, \Theta_n$. Once they are determined, $F_r(z)$ can be computed by (4.12) and (4.13) at any point in $\bar{D}$.

$H_r(z)$ should also be continuous in $\bar{D}$ in terms of the principal value of logarithmic function. Therefore, substituting (4.16), we change (4.12) to

$$\begin{aligned} G_r(z) + iH_r(z) &= \sum_{l=1}^{n} \left\{ \sum_{i=1}^{N_l-1} \left(\sum_{k=1}^{i} Q_{lk} \right) (\log(z - \zeta_{li}) - \log(z - \zeta_{l,i+1})) \right. \\ &\qquad \left. + \left(\sum_{k=1}^{N_l} Q_{lk} \right) \log(z - \zeta_{lN_l}) \right\} \\ &= \sum_{l=1}^{n} \sum_{i=1}^{N_l-1} \left(\sum_{k=1}^{i} Q_{lk} \right) \log \left(\frac{z - \zeta_{li}}{z - \zeta_{l,i+1}} \right) \end{aligned} \tag{4.17}$$

in the same manner as equation (4.7) and take its principal value. Then the linear equations (4.14) should be changed to

$$\begin{aligned} &\sum_{l=1}^{n} \sum_{i=1}^{N_l-1} \left(\sum_{k=1}^{i} Q_{lk} \right) \mathrm{Arg} \left(\frac{z_{mj} - \zeta_{li}}{z_{mj} - \zeta_{l,i+1}} \right) - \Theta_m = -\mathrm{Arg} z_{mj}, \\ &z_{mj} \in C_m, \quad j = 1, \ldots, N_m, \quad m = 1, \ldots, n. \end{aligned} \tag{4.18}$$

The formulation described above is summarized as follows.

Formulation RSLIT1. The approximate mapping function is given by

$$F_r(z) = z \exp(G_r(z) + iH_r(z)),$$

$$\begin{aligned} G_r(z) + iH_r(z) &= \sum_{l=1}^{n} \sum_{i=1}^{N_l-1} Q_l^i \, \mathrm{Log} \left(\frac{z - \zeta_{li}}{z - \zeta_{l,i+1}} \right) \\ &= \sum_{l=1}^{n} \sum_{i=1}^{N_l-1} Q_l^i \left\{ \log \left| \frac{z - \zeta_{li}}{z - \zeta_{l,i+1}} \right| + i \mathrm{Arg} \left(\frac{z - \zeta_{li}}{z - \zeta_{l,i+1}} \right) \right\}, \end{aligned}$$

where the unknown constants $Q_l^i = \sum_{k=1}^{i} Q_{lk}$, $i = 1, \ldots, N_l - 1$, $l = 1, \ldots, n$, and $\Theta_1, \ldots, \Theta_n$ are solutions of the $N_1 + \cdots + N_n$ simultaneous linear equations

$$\sum_{l=1}^{n} \sum_{i=1}^{N_l-1} Q_l^i \mathrm{Arg} \left(\frac{z_{mj} - \zeta_{li}}{z_{mj} - \zeta_{l,i+1}} \right) - \Theta_m = -\mathrm{Arg} z_{mj},$$

$$z_{mj} \in C_m, \quad j = 1, \ldots, N_m, \quad m = 1, \ldots, n.$$

If $C_1, \ldots, C_n$ are starlike with respect to their inside points $z_{10}, \ldots, z_{n0}$, also using (4.16) we can change (4.12) to

$$\begin{aligned} G_r(z) + iH_r(z) &= \sum_{l=1}^{n} \sum_{i=1}^{N_l} Q_{li} \log(z - \zeta_{li}) - \sum_{l=1}^{n} \sum_{i=1}^{N_l} Q_{li} \log(z - z_{l0}) \\ &= \sum_{l=1}^{n} \sum_{i=1}^{N_l} Q_{li} \log \left(\frac{z - \zeta_{li}}{z - z_{l0}} \right) \end{aligned} \tag{4.19}$$

in the same manner as equation (4.10) and take its principal value. The linear equations (4.14) should be changed to

$$\sum_{l=1}^{n}\sum_{i=1}^{N_l} Q_{li}\mathrm{Arg}\left(\frac{z_{mj}-\zeta_{li}}{z_{mj}-z_{l0}}\right)-\Theta_m=-\mathrm{Arg}z_{mj},$$

$$z_{mj}\in C_m,\quad j=1,\dots,N_m,\quad m=1,\dots,n. \tag{4.20}$$

Then another formulation can be obtained.

Formulation RSLIT2. The approximate mapping function is given by

$$F_r(z)=z\exp(G_r(z)+iH_r(z)),$$

$$\begin{aligned}G_r(z)+iH_r(z)&=\sum_{l=1}^{n}\sum_{i=1}^{N_l} Q_{li}\mathrm{Log}\left(\frac{z-\zeta_{li}}{z-z_{l0}}\right)\\&=\sum_{l=1}^{n}\sum_{i=1}^{N_l} Q_{li}\left\{\log\left|\frac{z-\zeta_{li}}{z-z_{l0}}\right|+i\mathrm{Arg}\left(\frac{z-\zeta_{li}}{z-z_{l0}}\right)\right\},\end{aligned}$$

where the unknown constants $Q_{11},Q_{12},\dots,Q_{nN_n}$ and $\Theta_1,\dots,\Theta_n$ are solutions of the $N_1+\cdots+N_n+n$ simultaneous linear equations

$$\sum_{l=1}^{n}\sum_{i=1}^{N_l} Q_{li}\mathrm{Arg}\left(\frac{z_{mj}-\zeta_{li}}{z_{mj}-z_{l0}}\right)-\Theta_m=-\mathrm{Arg}z_{mj},$$

$$z_{mj}\in C_m,\quad j=1,\dots,N_m,\quad m=1,\dots,n,$$

$$\sum_{i=1}^{N_l} Q_{li}=0,$$

$$l=1,\dots,n.$$

5. Numerical examples. The formulations CSLIT2 and RSLIT2 are applied to typical domains with curved boundaries. Some of them are taken from [5, 6] in which CSLIT1- and RSLIT1-like formulations were used.

Charge points as well as collocation points play an important role in the charge simulation method. It is still an open problem how to find their optimal arrangement. However, it is empirically known that the method can give numerical results of high accuracy if the charge point ζ_{li} is arranged on the outward normal of the boundary curve C_l at the corresponding collocation point z_{li} and near the boundary where collocation points are dense [1–6, 23]. In the numerical examples, we set $N_1=\cdots=N_n=N$, and the total number is nN.

The following indications are used for estimating computational errors:

$$E_{Ml}=\max_j\,||F_c(z_{l,j+1/2})|-R_l|, \tag{5.1}$$

$$E_{Rl}=|R_l-R_{dl}| \tag{5.2}$$

Downloaded 11/05/25 to 185.230.125.55 . Redistribution subject to SIAM license or copyright; see https://epubs.siam.org/terms-privacy

Downloaded 11/05/25 to 185.230.125.55 . Redistribution subject to SIAM license or copyright; see https://epubs.siam.org/terms-privacy

in the case of circular slit domains, and

$$E_{Al} = \max_j |\mathrm{Arg} F_r(z_{l,j+1/2}) - \Theta_l|, \tag{5.3}$$

$$E_{\Theta l} = |\Theta_l - \Theta_{dl}| \tag{5.4}$$

in the case of radial slit domains. The point $z_{l,j+1/2}$ is the middle point on C_l between z_{lj} and $z_{l,j+1}$, and R_{dl} and Θ_{dl} are obtained by doubling the number of simulation charges. When analytical solutions are known, R_l, R_{dl} and Θ_l, Θ_{dl} in the second terms of the right-hand side are replaced by r_l and θ_l, and the indication

$$E_{Fl} = \max_j \{|F(z_{lj}) - f(z_{lj})|,\ |F(z_{l,j+1/2}) - f(z_{l,j+1/2})|\} \tag{5.5}$$

is also presented. The functions $F(z)$ and $f(z)$ are for $F_c(z)$ and $f_c(z)$ or $F_r(z)$ and $f_r(z)$.

The computations were carried out on a AS4080/51GX (SUN SS10) workstation using programs coded in FORTRAN in double precision. The IMSL library was used for solving the simultaneous linear equations, and C_N is the L_1 condition number of the coefficient matrix.

Example 1. Exterior of a disk,

$$D : |z - z_0| > 1, \quad z_0 = 2.$$

The collocation points and the charge points are placed by

$$z_j = z_0 + \exp \frac{2(j-1)\pi i}{N}, \quad \zeta_j = z_0 + q \exp \frac{2(j-1)\pi i}{N},$$

where $0 < q < 1$ is a parameter. Analytical solutions

$$f_c(z) = \frac{z(z - z_0)}{z - (z_0 - 1/\bar{z}_0)}, \quad r = |z_0|,$$

$$f_r(z) = \frac{z(z - (z_0 - 1/\bar{z}_0))}{z - z_0}, \quad \theta = \arg z_0,$$

can be derived from [24, p. 340], where $\bar{z}_0$ is the complex conjugate of z_0. The latter can be changed to

$$f_r(z) = \exp(i\theta) \left\{ (z - z_0) \exp(-i\theta) + \frac{1}{(z - z_0) \exp(-i\theta)} + |z_0| + \frac{1}{|z_0|} \right\},$$

which is a Joukowski map with translation and rotation.

Figure 5.1 and Tables 5.1 and 5.2 show the numerical results. We can see typical features of the charge simulation method in the tables. As shown by E_F, high accuracy of the numerical mapping can be obtained. The accuracy of the radius R and the argument Θ of the slit is much higher. As q decreases from 1 to 0 and the charges move away from the boundary, the accuracy of the numerical results first increases and then decreases. On the other hand, the condition number C_N increases monotonically, and finally the coefficient matrix becomes numerically singular. The asterisk in the tables shows the ill conditioning. However, the approximate mapping functions are still analytical. The maximum modulus theorem tells us that the relative error

$$\begin{aligned} E_L(z) &= \left| \frac{F(z) - f(z)}{f(z)} \right| \\ &= |\exp\{G(z) + iH(z) - (g(z) + ih(z))\} - 1| \end{aligned}$$

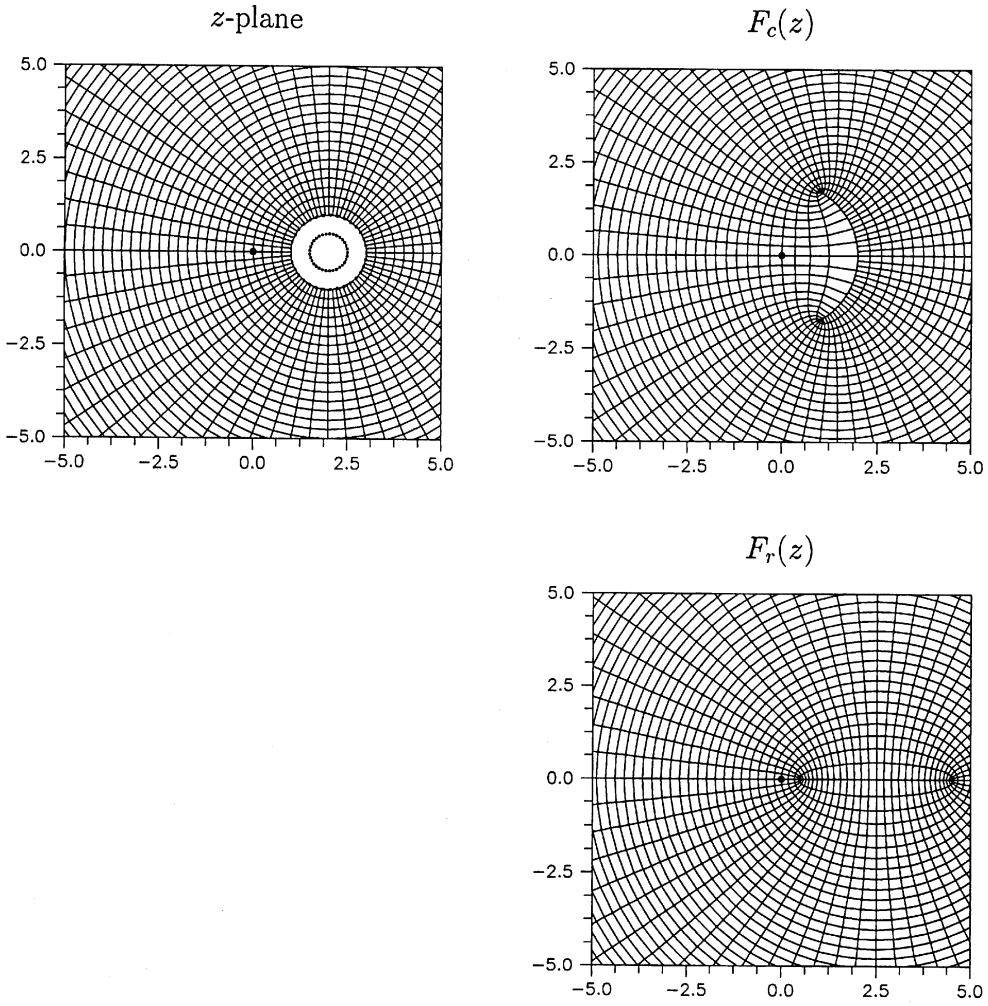

FIG. 5.1. *Numerical mapping, Example* 1.

TABLE 5.1
Numerical results, Example 1*, a circular slit,* $z_0 = 2$.

q	N	E_M	E_F	E_R	C_N
	17	1.8E–03	1.8E–03	9.0E–07	5.1E+06
0.2	33	3.8E–06	3.8E–06	1.5E–11	4.1E+12
	65	2.8E–07	3.2E–07	3.0E–09	6.0E+18*
	129	9.8E–07	9.8E–07	1.0E–08	1.4E+20*
	17	2.6E–03	2.6E–03	9.0E–07	2.7E+03
0.5	33	5.5E–06	5.5E–06	7.1E–12	1.4E+06
	65	4.4E–11	4.4E–11	4.4E–16	1.8E+11
	129	8.4E–13	9.0E–13	3.2E–14	6.4E+19*
	17	2.5E–02	2.5E–02	9.0E–07	5.4E+01
0.8	33	3.8E–04	3.8E–04	7.1E–12	6.3E+02
	65	1.5E–07	1.5E–07	4.4E–16	4.5E+04
	129	4.4E–14	4.5E–14	2.2E–16	1.1E+08

Downloaded 11/05/25 to 185.230.125.55 . Redistribution subject to SIAM license or copyright; see https://epubs.siam.org/terms-privacy

TABLE 5.2
Numerical results, Example 1*, a radial slit,* $z_0 = 2$.

q	N	E_A	E_F	E_Θ	C_N
	17	5.9E–04	2.7E–03	1.2E–15	7.7E+06
0.2	33	1.2E–06	5.5E–06	8.5E–12	6.0E+12
	65	3.2E–07	2.0E–06	7.9E–09	2.4E+19*
	129	4.5E–06	4.1E–05	3.7E–09	4.9E+20*
	17	1.3E–03	5.7E–03	1.8E–17	7.7E+03
0.5	33	2.7E–06	1.2E–05	2.3E–17	4.1E+06
	65	2.2E–11	9.9E–11	1.2E–17	5.2E+11
	129	5.6E–15	2.7E–14	1.6E–16	1.1E+19*
	17	7.1E–03	1.8E–02	1.8E–18	3.3E+02
0.8	33	8.2E–05	1.1E–04	9.0E–18	4.8E+03
	65	2.7E–08	3.1E–08	5.3E–18	3.8E+05
	129	8.4E–15	1.2E–14	1.7E–18	1.0E+09

takes its maximum value somewhere on the boundary because

$$\lim_{z\to\infty} E_L(z) = 0$$

in this method. The optimum value of q is small for small N and large for large N; i.e., the charges should be moved toward the boundary or away from the boundary when N increases or decreases. If q is fixed, accuracy of the numerical results together with the condition number exponentially increases as a function of N until the coefficient matrix becomes singular. We can find the rough relations

$$E_R \ll E_M \simeq E_F$$

and

$$E_\Theta \ll E_A \simeq E_F$$

which suggest that E_M and E_A of (5.1) and (5.3) can be expected to be reasonable estimates of the accuracy of the approximate mapping functions even if the analytical solutions are not known.

In the case of radial slit domains, if even numbers of simulation charges are used, the linear equations may be singular in a highly symmetrical situation. In fact, we can prove that the coefficient matrices of RSLIT1 and RSLIT2 are both singular in this example. Such a problem does not occur in the case of circular slit domains.

Example 2. Exterior of a Cassini's oval,

$$D : |(z - z_0)^2 - 1| > a^2, \quad z_0 = 2, \quad a = 1.02.$$

This is an example of the domain with nonconvex boundary curves. The collocation points are first placed by

$$z_j = z_0 + \alpha_j \exp(i\beta_j),$$
$$\alpha_j = \left\{\cos 2\beta_j + \left(\cos^2 2\beta_j + a^4 - 1\right)^{1/2}\right\}^{1/2}, \quad \beta_j = \frac{2(j-1)\pi i}{N}$$

at equal intervals in argument. Then, the charge points are placed by

$$\zeta_j = z_j + \frac{q}{2}\,|z_{j+1} - z_{j-1}| \exp\left\{i\left(\arg(z_{j+1} - z_{j-1}) + \frac{\pi}{2}\right)\right\}$$

Downloaded 11/05/25 to 185.230.125.55 . Redistribution subject to SIAM license or copyright; see https://epubs.siam.org/terms-privacy

Downloaded 11/05/25 to 185.230.125.55 . Redistribution subject to SIAM license or copyright; see https://epubs.siam.org/terms-privacy

TABLE 5.3
Numerical results, Example 2, *a circular slit,* $z_0 = 2$, $a = 1.02$.

N	q	E_M	E_F	E_R	C_N
17	0.5	1.9E–01	1.9E–01	3.0E–04	5.2E+01
33	0.5	4.8E–02	4.8E–02	1.3E–04	8.6E+01
	1	1.4E–02	1.4E–02	1.3E–05	8.4E+02
65	0.5	1.5E–02	1.5E–02	6.0E–05	1.6E+02
	1	8.9E–04	8.9E–04	2.8E–06	9.6E+02
	2	1.3E–04	1.3E–04	1.2E–07	1.9E+05
129	0.5	6.7E–03	6.7E–03	5.2E–05	3.1E+02
	1	2.5E–04	2.5E–04	8.1E–07	1.7E+03
	2	3.5E–07	3.5E–07	6.1E–10	7.9E+04
	4	1.0E–07	1.0E–07	7.7E–12	2.8E+10

TABLE 5.4
Numerical results, Example 2, *a radial slit,* $z_0 = 2$, $a = 1.02$.

N	q	E_A	E_F	E_Θ	C_N
17	0.5	1.8E–01	4.1E–01	1.4E–16	4.4E+02
33	0.5	2.3E–02	5.1E–02	3.7E–17	1.9E+03
	1	2.5E–02	6.4E–02	4.4E–17	1.7E+04
65	0.5	2.4E–03	5.2E–03	2.2E–17	7.5E+03
	1	3.3E–04	7.6E–04	1.3E–19	5.9E+04
	2	8.3E–04	2.3E–03	4.1E–17	2.1E+07
129	0.5	4.6E–04	1.5E–03	1.5E–17	3.1E+04
	1	3.5E–05	6.1E–05	1.2E–17	2.6E+05
	2	1.2E–07	2.7E–07	1.3E–17	7.0E+07
	4	1.5E–06	4.2E–06	1.1E–15	4.4E+13

outside the domain in a similar way as described in [4]. The parameter $q > 0$, which has a different meaning from that in the previous example, is called the *assignment factor*. Consequently, ζ_j lies on the outward normal at z_j and nears the boundary where collocation points are dense.

Analytical solutions

$$f_c(z) = a\frac{z^*(z^* - z_0^*)}{z^* - (z_0^* - 1/\bar{z}_0^*)}, \quad r = a|z_0^*|,$$
$$f_r(z) = a\frac{z^*(z^* - (z_0^* - 1/\bar{z}_0^*))}{z^* - z_0^*}, \quad \theta = \arg z_0^*,$$
$$z^* = \frac{\sqrt{(z - z_0)^2 - 1}}{a} + z_0^*, \quad z_0^* = -\frac{\sqrt{(-z_0)^2 - 1}}{a}$$

can be derived using $f_c(z)$ and $f_r(z)$ of Example 1 and $f(z) = \sqrt{z^2 - 1}/a$ which maps the exterior of a Cassini's oval $|z^2 - 1| > a^2$ onto the exterior of the unit disk under the conditions $f(\infty) = \infty$ and $f'(\infty) > 0$. In this example, $r = \sqrt{3}$ and $\theta = 0$ for $z_0 = 2$.

Figure 5.2 and Tables 5.3 and 5.4 show the numerical results. Without reentrant corners, the concavity of the boundary curve presents no severe difficulty. We can see typical features of the method also in this example. Note that the charges lie, roughly speaking, on a same virtual curve when the ratio N/q is kept constant, and note that they may collide with each other to cause the singularity of the coefficient matrix when $N/q < 33$.

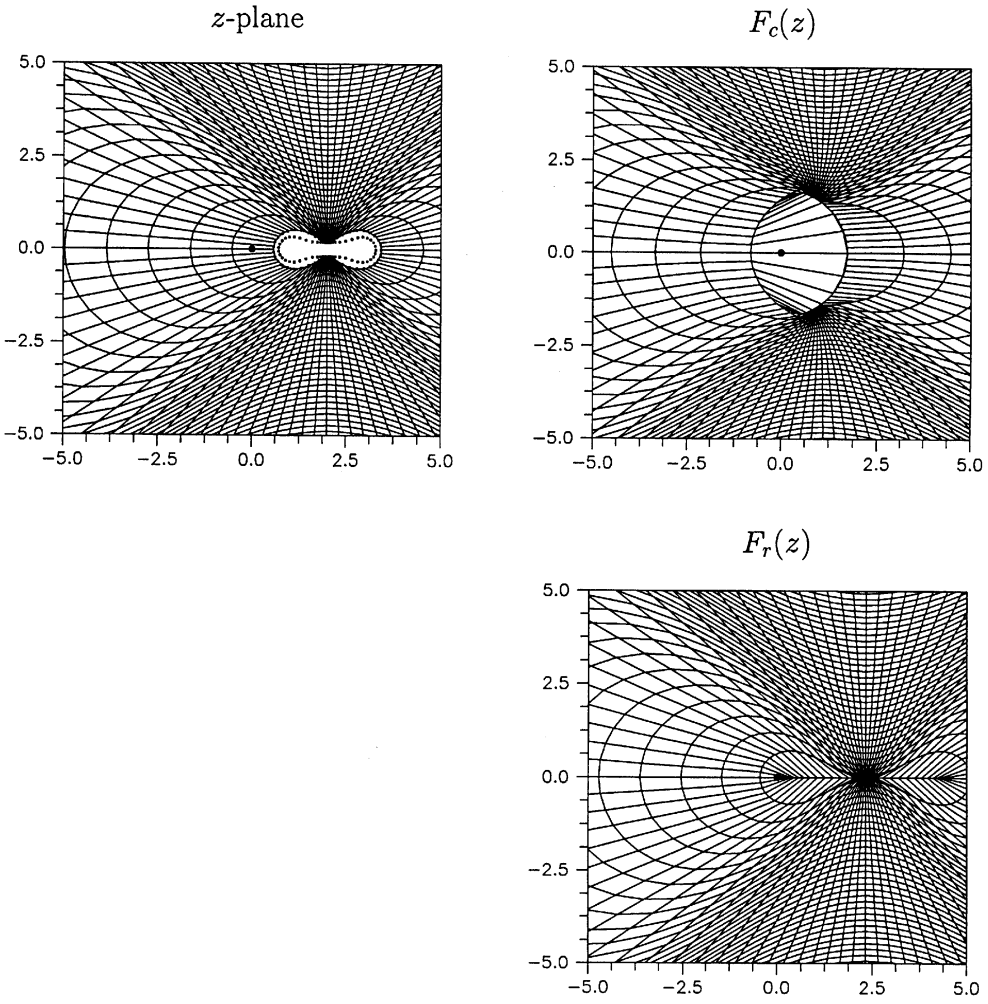

FIG. 5.2. *Numerical mapping, Example* 2.

Example 3. Exterior of three disks with different radii,

$$D : |z - z_{l0}| > \rho_l, \quad z_{l0} = 2 \exp \frac{2(l-1)\pi i}{3}, \quad l = 1, 2, 3,$$

$$\rho_1 = 1, \quad \rho_2 = 0.5, \quad \rho_3 = 1.5.$$

The collocation points and the charge points are placed by

$$z_{lj} = z_{l0} + \rho_l \exp \frac{2(j-1)\pi i}{N}, \quad \zeta_{lj} = z_{l0} + q\rho_l \exp \frac{2(j-1)\pi i}{N}.$$

Analytical solutions are not known, and the problem has no symmetry.

Figure 5.3 and Tables 5.5 and 5.6 show the numerical results. The values of R and Θ are shown until a nonzero digit appears in the right-hand side of (5.2) and (5.4). High accuracy can be obtained also in this example. The maximum errors estimated by E_M and E_A appear on the third circle with the largest radius.

Downloaded 11/05/25 to 185.230.125.55 . Redistribution subject to SIAM license or copyright; see https://epubs.siam.org/terms-privacy

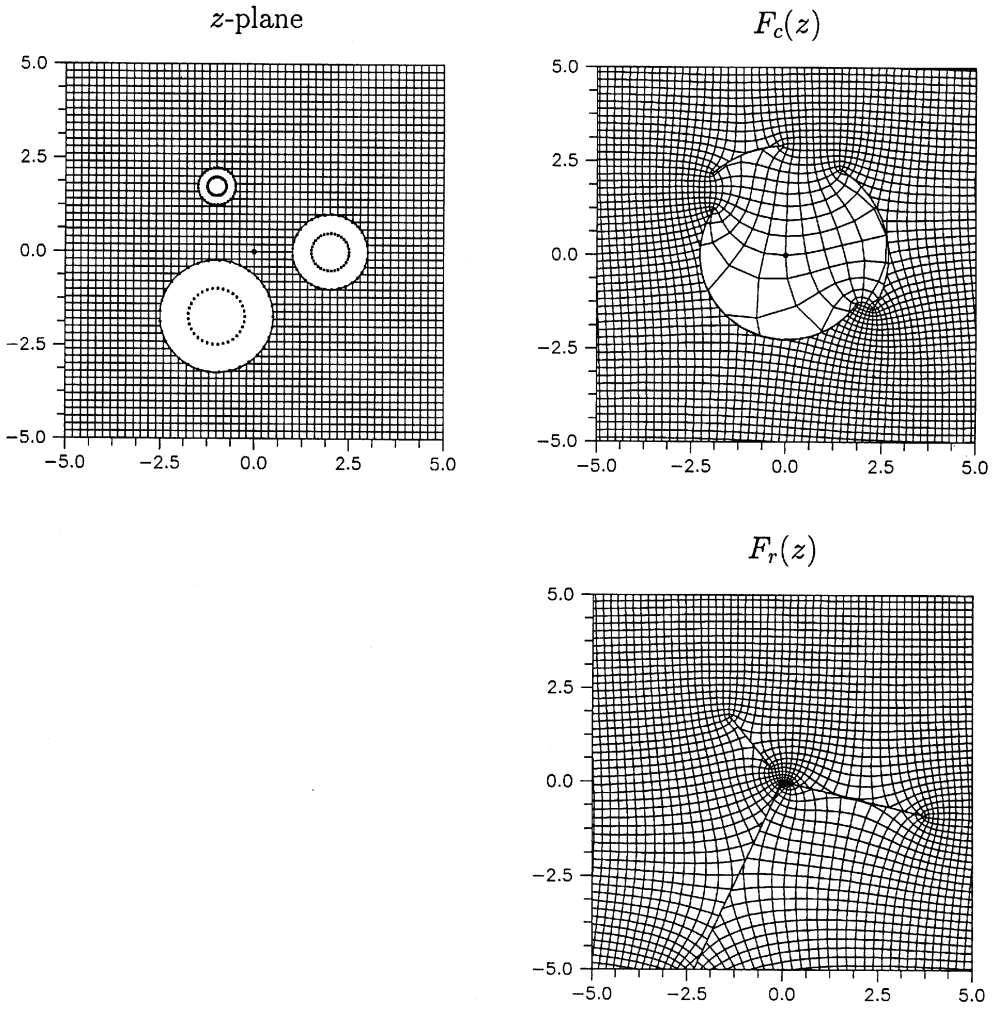

FIG. 5.3. *Numerical mapping, Example* 3.

TABLE 5.5
Numerical results, Example 3*, three circular slits,* $q = 0.8$.

N		E_M	E_R	R	C_N
	S_{c1}	2.7E–02	2.7E–03	2.693	
17	S_{c2}	5.2E–03	1.8E–03	2.910	2.0E+02
	S_{c3}	1.2E–01	1.3E–03	2.264	
	S_{c1}	4.3E–04	3.8E–05	2.69581	
33	S_{c2}	7.6E–05	4.9E–05	2.91213	2.3E+03
	S_{c3}	1.5E–02	7.6E–06	2.265366	
	S_{c1}	1.7E–07	1.4E–08	2.69585239	
65	S_{c2}	3.0E–08	1.8E–08	2.91217883	1.7E+05
	S_{c3}	4.6E–05	5.2E–09	2.265373690	
	S_{c1}	5.8E–14			
129	S_{c2}	8.5E–14			4.2E+08
	S_{c3}	4.5E–09			

Downloaded 11/05/25 to 185.230.125.55 . Redistribution subject to SIAM license or copyright; see https://epubs.siam.org/terms-privacy

Downloaded 11/05/25 to 185.230.125.55 . Redistribution subject to SIAM license or copyright; see https://epubs.siam.org/terms-privacy

TABLE 5.6
Numerical results, Example 3, three radial slits, $q = 0.8$.

N		E_A	E_Θ	Θ	C_N
	S_{r1}	8.6E–03	4.6E–04	–0.2363	
17	S_{r2}	1.1E–03	6.8E–04	2.2474	4.0E+02
	S_{r3}	5.0E–02	6.4E–05	–2.00509	
	S_{r1}	9.7E–05	1.3E–05	–0.23584	
33	S_{r2}	1.4E–05	9.8E–06	2.246740	5.4E+03
	S_{r3}	5.9E–03	4.1E–06	–2.005022	
	S_{r1}	3.3E–08	4.0E–09	–0.235829745	
65	S_{r2}	5.5E–09	3.1E–09	2.246730515	4.3E+05
	S_{r3}	1.8E–05	1.3E–09	–2.005025892	
	S_{r1}	1.5E–14			
129	S_{r2}	2.4E–13			1.1E+09
	S_{r3}	1.8E–09			

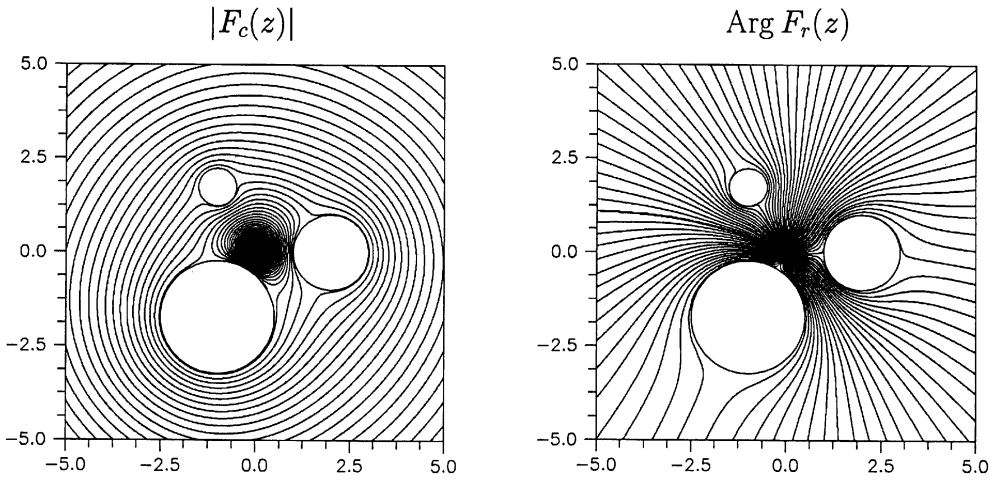

FIG. 5.4. *Contour lines of* $|F_c(z)|$ *and* $\mathrm{Arg}F_r(z)$*, Example* 3.

Figure 5.4 shows the contour lines of $|F_c(z)|$ and $\mathrm{Arg}F_r(z)$. They are streamlines of a two-dimensional vortex flow and a point-source flow with obstacles. A vortex or a point source is at the origin, and the disks mean cross sections of the cylindrical objects.

If the disks are of the same radius $\rho_1 = \rho_2 = \rho_3 = 1$, then $\theta_1 = 0$, $\theta_2 = 2\pi/3$, and $\theta_3 = -2\pi/3$ from the symmetry of rotation. The accuracy of the numerical mapping estimated by E_M and E_A is, roughly speaking, of the same order of magnitude as in the first example. We have also confirmed that the method works well when the boundary circles are replaced by ellipses.

6. Concluding remarks. A unified numerical method has been presented for computing the following two conformal maps: (a) from a domain exterior to closed Jordan curves onto a circular slit domain and (b) from a domain exterior to closed Jordan curves onto a radial slit domain. The former is important in problems of two-dimensional vortex flow with obstacles, and the latter is important in problems of two-dimensional point-source flow with obstacles. They constitute a dual problem and can be computed in a dual way. Such a method of numerical mapping has not been proposed previously. The method in which a pair of conjugate harmonic functions

are approximated by a linear combination of complex logarithmic potentials without integration is quite simple and easy to program. It is suited for mapping of domains with curved boundaries. The effectiveness of the method has been demonstrated by some typical examples in the preceding section, where the formulations CSLIT2 and RSLIT2 are used. Almost the same results can be obtained using the formulations CSLIT1 and RSLIT1.

In the case of radial slit domains, if even numbers of simulation charges are used, the simultaneous linear equations to be solved may be singular in a highly symmetrical situation. However, this does not prevent the use of the method in practice. We have only to use odd numbers of simulation charges. Such a problem does not occur in the case of circular slit domains.

The fundamentals of the mapping method proposed here are feasible with Symm-like integral equations. We expect that an integral equation reformulation of the method is effective to overcome the difficulties associated with reentrant corners.

REFERENCES

[1] K. Amano, *Numerical conformal mapping based on the charge simulation method*, Trans. Inform. Process. Soc. Japan, 28 (1987), pp. 697–704 (in Japanese).

[2] K. Amano, *Numerical conformal mapping of exterior domains based on the charge simulation method*, Trans. Inform. Process. Soc. Japan, 29 (1988), pp. 62–72 (in Japanese).

[3] K. Amano, *Numerical conformal mapping of doubly-connected domains by the charge simulation method*, Trans. Inform. Process. Soc. Japan, 29 (1988), pp. 914–924 (in Japanese).

[4] K. Amano, *A charge simulation method for the numerical conformal mapping of interior, exterior and doubly-connected domains*, J. Comput. Appl. Math., 53 (1994), pp. 353–370.

[5] K. Amano, *Numerical conformal mapping onto the circular slit domains*, Trans. Inform. Process. Soc. Japan, 36 (1995), pp. 219–225 (in Japanese).

[6] K. Amano, *Numerical conformal mapping onto the radial slit domains by the charge simulation method*, Trans. Japan SIAM, 5 (1995), pp. 267–280 (in Japanese).

[7] J. P. Berrut, *A Fredholm integral equation of the second kind for conformal mapping*, J. Comput. Appl. Math., 14 (1986), pp. 99–110.

[8] G. Fairweather and R. L. Johnston, *The method of fundamental solutions for problems in potential theory*, in Treatment of Integral Equations by Numerical Methods, C. T. H. Baker and G. F. Miller, eds., Academic Press, London, 1982, pp. 349–359.

[9] D. Gaier, *Konstruktive Methoden der konformen Abbildung*, Springer, Berlin, 1964.

[10] D. Gaier, *Integralgleichungen erster Art und konforme Abbildung*, Math. Z., 147 (1976), pp. 113–129.

[11] D. Gaier, *Das logarithmische Potential und die konforme Abbildung mehrfach zusammenhängender Gebiete*, in E. B. Christoffel, The Influence of his Work on Mathematics and the Physical Sciences, P. L. Butzer and F. Fehér, eds., Birkhäuser, Basel, 1981, pp. 290–303.

[12] J. K. Hayes, D. K. Kahaner, and R. G. Kellner, *An improved method for numerical conformal mapping*, Math. Comp., 26 (1972), pp. 327–334.

[13] P. Henrici, *Fast Fourier methods in computational complex analysis*, SIAM Rev., 21 (1979), pp. 481–527.

[14] P. Henrici, *Applied and Computational Complex Analysis, Vol.* 3, Wiley, New York, 1986.

[15] D. M. Hough and N. Papamichael, *The use of splines and singular functions in an integral equation method for conformal mapping*, Numer. Math., 37 (1981), pp. 133–147.

[16] D. M. Hough and N. Papamichael, *An integral equation method for the numerical conformal mapping of interior, exterior and doubly-connected domains*, Numer. Math., 41 (1983), pp. 287–307.

[17] M. Katsurada, *A mathematical study of the charge simulation method* II, J. Fac. Sci. Univ. Tokyo Sect. IA Math., 36 (1989), pp. 135–162.

[18] M. Katsurada, *Asymptotic error analysis of the charge simulation method in a Jordan region with an analytic boundary*, J. Fac. Sci. Univ. Tokyo Sect. IA Math., 37 (1990), pp. 635–657.

[19] M. Katsurada, *Charge simulation method using exterior mapping functions*, Japan J. Indust. Appl. Math., 11 (1994), pp. 47–61.

[20] M. Katsurada and H. Okamoto, *A mathematical study of the charge simulation method* I, J. Fac. Sci. Univ. Tokyo Sect. IA Math., 35 (1988), pp. 507–518.

Downloaded 11/05/25 to 185.230.125.55 . Redistribution subject to SIAM license or copyright; see https://epubs.siam.org/terms-privacy

[21] T. Kitagawa, *On the numerical stability of the method of fundamental solution applied to the Dirichlet problem*, Japan J. Appl. Math., 5 (1988), pp. 123–133.
[22] R. Mathon and R. L. Johnston, *The approximate solution of elliptic boundary-value problems by fundamental solutions*, SIAM J. Numer. Anal., 14 (1977), pp. 638–650.
[23] S. Murashima, *Charge Simulation Method and its Application*, Morikita, Tokyo, 1983 (in Japanese).
[24] Z. Nehari, *Conformal Mapping*, McGraw-Hill, New York, 1952.
[25] H. Okamoto and M. Katsurada, *A rapid solver for the potential problems*, Bull. Japan SIAM, 2 (1992), pp. 2–20 (in Japanese).
[26] L. Reichel, *A fast method for solving certain integral equations of the first kind with application to conformal mapping*, J. Comput. Appl. Math., 14 (1986), pp. 125–142.
[27] G. T. Symm, *An integral equation method in conformal mapping*, Numer. Math., 9 (1966), pp. 250–258.
[28] G. T. Symm, *Numerical mapping of exterior domains*, Numer. Math., 10 (1967), pp. 437–445.
[29] G. T. Symm, *Conformal mapping of doubly-connected domains*, Numer. Math., 13 (1969), pp. 448–457.
[30] L. N. Trefethen, ed., *Numerical Conformal Mapping*, North–Holland, Amsterdam, 1986.

Downloaded 11/05/25 to 185.230.125.55 . Redistribution subject to SIAM license or copyright; see https://epubs.siam.org/terms-privacy